Surface Tension and Surface Roughness of Supported Polystyrene Films

Laurence Lurio,*,† Hyunjung Kim,‡,§,⊥ Adrian Rühm,# Joydeep Basu,‡,& Jyotsana Lal,^ Sunil Sinha,‡,§ and Simon G. J. Mochrie%

Department of Physics, Northern Illinois University, DeKalb, Illinois 60115; Advanced Photon Source, Argonne National Laboratory, Argonne, Illinois 60439; Department of Physics, University of California San Diego, La Jolla, California 92093; Department of Physics, Sogang University, Seoul 121-724, Korea; Center for Materials Science and Engineering, Massachusetts Institute of Technology, Cambridge, Massachusetts 02139; Materials Research Laboratory, University of Illinois Urbana-Champaign, Urbana, Illinois 61801; IPNS, Argonne National Laboratory, Argonne, Illinois 60439; and Department of Physics, Yale University, New Haven, Connecticut 06520

Received February 13, 2003; Revised Manuscript Received May 12, 2003

ABSTRACT: Surface-diffuse X-ray scattering has been measured from a series of polystyrene (PS) films supported on oxide-terminated Si substrates. Films of thicknesses ranging from 84 to 359 nm were investigated over a temperature range from 120 to 180 °C, all above the bulk PS glass transition temperature. The surface tension was extracted from the absolute intensity of diffuse scattering. The values show a slight excess of the surface tension (∼20%) over the bulk material. Capillary wave theory is used to describe the observed diffuse scattering down to in-plane length scales of 2 nm, the limit of our resolution. The total surface roughness exceeds the value that would be expected from capillary wave theory, indicating the presence of excess roughness at length scales less than 2 nm.

Introduction

Polymer thin films are of great current interest both for basic scientific reasons and on account of their importance in a variety of technological applications including optical coatings, adhesives, biocompatible surfaces for medical implants, computer disk drives, sensor films, and electronic packaging materials. Surface roughness is a critical parameter in many of these applications. The study of surface roughness also provides a window through which to observe the physics internal to the film. The surface roughness of thin polymer films is influenced by properties such as surface tension, viscosity, van der Waals interactions with the substrate, and the molecular scale structure of the polymer.

In simple bulk liquids the roughness of the liquid−vapor interface is chiefly determined by thermally excited capillary waves. The total surface roughness results from the integration of these excitations from wavelengths on the order of the molecular size up to a long wavelength cutoff determined by gravity. The typical surface roughness is on the order of half a nanometer. Thermal capillary-wave roughness has been studied on a number of liquids, such as water,[1,2] helium,[3] and hydrocarbons,[4,5] and it has also been the subject of a recent comprehensive review by Penfold.[6] Capillary waves also play the dominant role in determining the surface morphology of polymer films. In this case a number of factors peculiar to polymers and the film geometry become important. In the film geometry, van der Waals interactions between the polymer and the substrate replace gravity as the dominant force damping long-wavelength capillary modes. This reduces the length scales over which capillary wave roughness is observed and leads to a strong thickness and substrate composition dependence of the surface roughness. The short length-scale modes of the capillary wave spectrum may also be cut off at length scales significantly greater than the monomer size. This may result from the effects of bending rigidity[7,8] from the highly viscous state of the polymer which can couple chain stretching in the polymer to capillary modes[9] or from short-range intermolecular forces which can modify the surface tension.[10] In addition, the local structure of the polymer itself may lead to an intrinsic roughness at the surface, unrelated to capillary waves.

One well-established method for characterizing surface roughness down to atomic length scales is surface-diffuse X-ray scattering.[1,11−13] The intensity of surface-diffuse X-ray scattering is related to the Fourier transform of the surface-height correlation function. Consequently, this technique can yield information not only about the total surface roughness but also about how the spectrum of roughness depends on length scale. For solid surfaces scanning probe microscopes are frequently employed to measure this spectrum, but these tools are not able to probe liquid surfaces without disturbing them. Light scattering has also been successfully applied to bulk liquid surfaces. Light scattering cannot be used to probe the equilibrium surface roughness for thin viscous films, however, since the capillary modes accessible to light scattering are of such a large lateral wavelength as to be frozen in place by viscosity. Neutron scattering has advantages for heterogeneous polymer films since the contrast can be tuned by selective deuteration; nevertheless, the higher brilliance of synchrotron X-ray sources provides an advantage for measuring the low intensities associated with surface-diffuse scattering.

† Northern Illinois University.
‡ Argonne National Laboratory.
§ University of California San Diego.
⊥ Sogang University.
Massachusetts Institute of Technology.
& University of Illinois Urbana−Champaign.
^ IPNS, Argonne National Laboratory.
% Yale University.
$ Present address: Max-Planck-Institut für Metallforschung, Stuttgart, Germany.
* Corresponding author: e-mail lurio@physics.niu.edu.

10.1021/ma034189l CCC: $25.00
Published on Web 06/27/2003

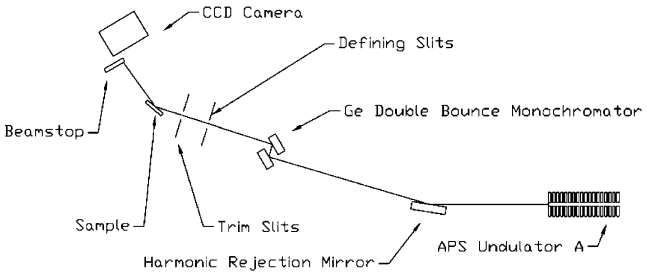

Figure 1. Layout of beamline at sector 8 of the APS.

A number of experiments have been performed to measure the surface roughness of polymer films, and these have been recently reviewed in a book by Tolan.[14] In particular, Wang and collaborators[15] measured X-ray scattering from supported films of PS on silicon substrates. Their results indicated that long-wavelength capillary modes were suppressed by van der Waals interactions with the substrate. They also found deviations from the expected form of scattering at large wavevectors. Surface roughness was expected to modify the exponent of the decay of the diffuse scattering as a function of in-plane wavevector, and they did not find this modification. Wang et al. attribute this to an increased surface tension at short length scales. However, this result remains puzzling since it has no theoretical motivation. In the experiments of Wang et al. the films were annealed at temperatures above the glass transition temperature but measured at room temperature, and this may have effected the surface properties.

In the present measurements we have employed surface-diffuse X-ray scattering to probe the roughness of thin PS films supported on silicon substrates. Films were measured in situ over a range of temperatures (120−180 °C) above the glass transition temperature (T_g = 97.2 °C[16] at a molecular weight of 123K). To evaluate absolute scattering cross sections and compare them to theory, data were normalized by comparison with two independent intensity standards. From these measurements we demonstrate that a range of wavevectors exist over which the surface roughness is well described by capillary wave theory. Moreover, we find a surface tension close to the accepted bulk values for PS.

Experimental Section

Polymer films were prepared by dissolving PS of molecular weight 123 000 g/mol and $M_w/M_n = 1.08$ in toluene and then spin-casting them onto optically flat silicon substrates. The silicon substrates were 14 mm × 14 mm × 0.5 mm and possessed a native oxide layer typically ∼2 nm thick. After spin-casting samples were annealed in a vacuum for 12 h at 150 °C to ensure complete solvent removal. Films of varying thickness were prepared by varying the concentration of PS in toluene and then spin-casting at constant angular velocity (ω = 2500 rpm). Thickness was empirically determined to depend on concentration as $d = 2.3C^{1.26}$, where d is the film thickness in nm and C the concentration in mg of PS/mL of solvent. The thicknesses of the PS films investigated ranged from 84 to 359 nm. For the X-ray measurements, films were mounted in a temperature-controlled sample chamber whose vacuum space (∼10^{-3} Torr) was integrated with the vacuum of the X-ray beamline. The sample temperature could be controlled from room temperature to 180 °C. Above 180 °C the samples were found to degrade.

Figure 1 portrays the scattering geometry. The incident beam was generated by the first harmonic of an APS undulator A with an 18 mm gap yielding a first harmonic energy centered at 7.665 keV. Higher harmonics of the undulator were removed by reflection at 0.15° from a flat Si mirror 29.2 m from the X-ray source point. A Germanium channel-cut double-bounce monochromator located 64.4 m from the source and 1855 mm from the sample selected a narrow energy slice ($\Delta E/E \gg 3 \times 10^{-4}$) from the undulator harmonic. The beam was collimated to 200 × 200 μm^2 in the vertical and horizontal directions using a set of crossed in-vacuum slits 640 mm from the sample. The scatter from this set of slits was removed by trim slits 165 mm in front of the sample. The surface-diffuse scattering was measured using a Princeton Instruments CCD camera located 316 mm behind the sample. The camera consisted of a fluorescent screen coupled to a 1256 × 1152 pixel array via a 2.4:1 tapered capillary fiber. The effective CCD pixel size was 0.054 mm × 0.054 mm, corresponding to an angular resolution of 171 μrad. The X-rays specularly reflected from the polymer surface were intercepted by a beamstop just in front of the CCD camera, but still inside the evacuated detector arm. This prevented any stray scattering that would result from the specular beam impinging on the 0.25 mm thick Kapton exit window. The beamstop was equipped with a PIN diode current integrating detector used to measure the direct beam intensity. Direct beam intensity measurements were made by translating the sample out of the beam and then translating the beamstop from the specular to the direct beam position. Diffuse-scattering measurements were placed on an absolute intensity scale by comparing the intensity of the direct beam intercepted on the PIN diode with the diffuse intensity measured on the CCD camera. The detector/PIN diode configuration was calibrated by reference to an amorphous carbon calibrated small-angle X-ray scattering (SAXS) standard. This procedure was accurate to within approximately 10% in absolute intensity, as verified by cross-calibration against an independent polyethylene intensity standard. The sample surface was oriented so that specular reflection deflected the beam horizontally. Films were thin and viscous enough to be unaffected by the wafer orientation. By arranging for the X-ray incidence angle (0.14°) to lie below the critical angle for total external reflection (0.16°), the X-ray penetration into the film was restricted to a depth of 9 nm. Consequently, scattering from the film−substrate interface as well as bulk scattering from within the film and from the substrate was small. Measurements were also taken at angles of incidence above the PS critical angle in order to quantify the contribution to the scattering from the bulk PS.

Scattering Theory

In the limit of the distorted wave Born approximation the diffuse X-ray scattering from an interface is given by[11]

$$\frac{d\sigma}{d\Omega} = \rho_e^2 r_e^2 A_{xy} |T(\alpha)|^2 |T(\beta)|^2 S(\mathbf{q}) \qquad (1)$$

Here ρ_e is the average electron density, A_{xy} is the illuminated interface area, r_e is the classical electron radius, $T(\theta)$ is the Fresnel transmission coefficient, $\boldsymbol{q} = \boldsymbol{k}_{out} - \boldsymbol{k}_{in}$ is the wavevector transfer, $S(\boldsymbol{q})$ is the structure factor, and α and β are grazing angle of incidence and scattering, respectively. For an isotropic rough surface the structure factor depends on the surface height−height correlation function $g(R) = \langle [h(R) - h(0)]^2 \rangle$ and is given by

$$S(\mathbf{q}) = \frac{1}{q_z^2} \int_0^\infty J_0(q_R R) \exp[-q_z^2 g(R)/2] 2\pi R \, dR \qquad (2)$$

Here $R = (x^2 + y^2)^{1/2}$ is the separation in the plane of the surface, q_z is the component of the wavevector transfer normal to the surface, and q_R is the in-plane component of the wavevector transfer. McClain et al.[7]

derived a form for $g(R)$ resulting from surface capillary waves. For the range of wavevectors $q_R < q_u$ this form is well approximated by

$$g(R) = B\left[\ln(e^{\gamma_e} q_u/2\pi) + \frac{1}{2}\ln\left(R^2 + \frac{4\pi^2}{{q_u}^2}\right)\right] + 2{\sigma_0}^2 \quad (3)$$

Here $B = k_B T/\pi\gamma$, γ is the surface tension at temperature T, k_B is Boltzmann's constant, $\gamma_e \gg 0.5772$ is Euler's constant, and q_u is an upper wavevector cutoff. We have added an additional term σ_0, which represents intrinsic roughness or diffuseness of the interface. This might, for example, correspond to the shape of the molecule at the surface. At very small wavevectors eq 3 would have to be modified to include modifications due to van der Waals forces from the substrate.[7] The present measurement does not extend down to such small wavevectors. Equation 2 can now be integrated.[17] One obtains for $\eta < 2$

$$S(q) \approx \frac{2\pi}{{q_z}^2}\exp(-{\sigma_0}^2 {q_z}^2)\left(\frac{4\pi}{q_u e^{\gamma_e}}\right)^{\eta}\left(\frac{q_R}{2}\right)^{\eta/2-1}\left(\frac{2\pi}{q_u}\right)^{1-\eta/2} \times \frac{K_{1-\eta/2}(2\pi q_R/q_u)}{\Gamma(\eta/2)} \quad (4)$$

Here Γ is the gamma function, K is the modified Bessel function, and $\eta = B{q_z}^2/2$. If the result is expanded to second order in q_R/q_u, then eq 4 can be simplified to yield

$$S(q) \approx \frac{4\pi}{{q_z}^2 {q_R}^2}\exp(-\sigma^2 {q_z}^2)\left(\frac{q_R}{q_u e^{\gamma_e}}\right)^{\eta}\left\{\frac{\Gamma(1-\eta/2)}{\Gamma(\eta/2)} + \left(\frac{\pi q_R}{q_u}\right)^2\left[\frac{\Gamma(1-\eta/2)}{\Gamma(1+\eta/2)} - \left(\frac{\pi q_R}{q_u}\right)^{-\eta}\frac{1}{1-\eta/2}\right]\right\} \quad (5)$$

This expression is identical to the result obtained by Sinha et al.[11] with the exception of the terms of order $(q_R/q_u)^2$. These result from the large q cutoff in eq 3.

Previous authors such as Sanyal et al.,[5] Wang et al.,[15] and McClain et al.[7] integrate eq 2 over one of the in-plane dimensions in q_R in order to account for broad experimental resolution in the direction perpendicular to the scattering plane. We do not do this in the present analysis since we use a CCD with good resolution in both spatial directions.

In the limit of very small q_z, eq 5 simplifies to

$$S(q) \approx \frac{k_B T}{\gamma {q_R}^2} \quad (6)$$

We do not use this form in the fits to the data, but rather the full form of eq 5. Equation 6 is introduced in order to point out the connection between the intensity of the scattering and the magnitude of the surface tension. This is the primary basis of the present experiment's sensitivity to the surface tension.

The scattering geometry is shown in Figure 2. The z-axis is normal to the surface of the film, the x-axis is along the in-plane component of the incident wavevector, and the y-axis satisfies $\hat{\mathbf{y}} = \hat{\mathbf{z}} \times \hat{\mathbf{x}}$. The resolution is set by the length of the sides of the CCD pixels, $U = 0.054$ mm. This gives, in the small angle limit for α and β, $\Delta q_x \approx kUr \sin(\beta + \phi) = 10^{-4}$ nm^{-1} and $\Delta q_y \approx kU/r = 6.6 \times 10^{-3}$ nm^{-1}. The resolution in the y-direction is coarser than in the x-direction, but both are typically smaller than the smallest in-plane wavevector accessed, ~ 0.01 nm^{-1}. Consequently, resolution broadening will not affect the analysis of the data.

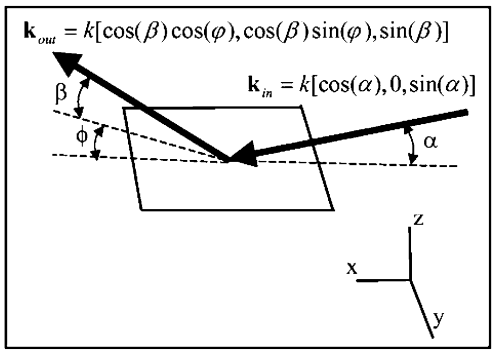

Figure 2. Experimental scattering geometry.

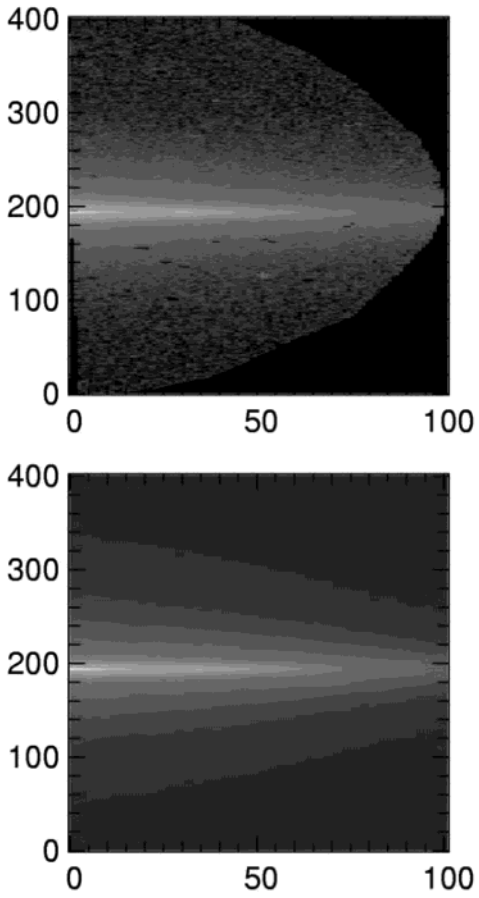

Figure 3. (top) Measured scattering from a 359 nm thick PS film on Si at 160 °C. The black areas were masked by the walls of the detector arm vacuum chamber and were excluded from the fits. (bottom) Theoretical model of the scattering as discussed in the text. The intensity is plotted on a logarithmic scale with the axis numbers corresponding to the binned pixel index of the CCD camera.

Results

The top panel of Figure 3 shows a two-dimensional scattering pattern obtained from a 359 nm film held at 160 °C. Figure 4 depicts cross sections through this scattering pattern at fixed columns, corresponding to nearly constant values of q_x. Note that since q_x and q_z are coupled, q_z is also different for each section. In the cross sections, each point represents the intensity from several pixels of the CCD binned together to improve

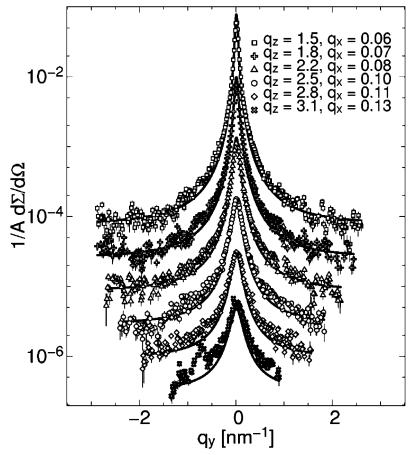

Figure 4. Cross sections of the diffuse scattering along data columns corresponding to a varying *y*-component of the in-plane wavevector transfer for several different values of q_z and q_x. The sample is a 359 nm thick PS film on Si at 160 °C. The solid lines represent the fits described in the text. Successive data sets have been multiplied by $^1/_3$ for clarity.

statistics. The binning was done asymmetrically in the *x*- and *y*-directions so as to give approximately uniform in-plane resolution. At small values of q_R the data fall off as $1/q_R^2$ as expected on the basis of eq 5. The diffuse scattering data fall off monotonically with q_z, consistent with exponential falloff with η predicted in eq 5. At larger values of q_R the data asymptote to a constant. This last effect is not a prediction of the capillary wave theory, and we will argue that it is due to bulk scattering within the PS film.

Shown in the lower panel of Figure 3 and as the solid lines in Figure 4 are the best fits to the data determined by least-squares minimization using eq 5. In the two-dimensional fits an additional constant background term was also added. The overall intensity was not varied since it is by the magnitude of the overall intensity that the surface tension is extracted. The parameters that were varied included the upper q cutoff, q_u, the surface tension, γ, the intrinsic roughness, σ_0, and a constant background. An additional parameter, of no physical significance, was the tilt of the sample relative to the horizontal. The overall values of χ^2 for the fits ranged between 8 and 10, except for the 120 °C and 180 °C data where it was a factor of 2 larger. Values of χ^2 that are significantly greater than unity indicate that the deviations between the fit and data are dominated by systematic rather than statistical errors. Close inspection of the fits shows that the dependence of the falloff of the intensity with q_y deviates from the theoretical model at large values of q_y and that the curvature of the fits is slightly different than the curvature of the experimental data. This deviation could be a sign that the surface roughness at the largest in-plane wavevectors may not be well described by capillary wave theory. An alternate possibility is that the background term, assumed to be independent of q, may, in fact, be q dependent. There will also be experimental sources of systematic errors, and these will strongly influence χ^2 whenever the statistical variation in photon counts become very small. These include factors such as the calibration of the absolute intensity, variations in the sensitivity of the CCD camera over its face, or distortion of the CCD image due to the optical fibers (although this distortion was calibrated and corrected to first order). Inspection of the fits shows, however, that

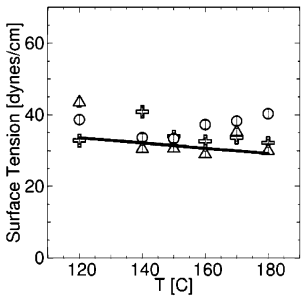

Figure 5. Surface tension vs temperature for different film thicknesses: cross, 86 nm; triangle, 142 nm; circle, 359 nm. The solid line is the bulk PS surface tension.

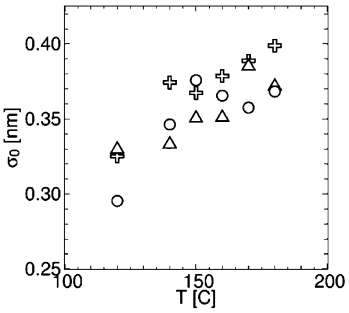

Figure 6. Intrinsic roughness vs film thickness and temperature: cross, 86 nm; triangle, 142 nm; circle, 359 nm.

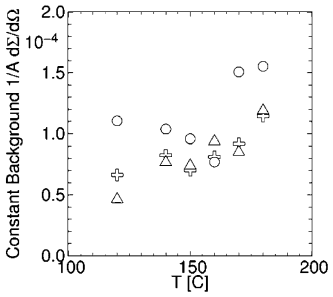

Figure 7. Constant background vs temperature and film thickness: cross, 86 nm; triangle, 142 nm; circle, 359 nm. The error bars obtained from least-squares minimization are smaller than the points.

over most of the range of wavevectors the model does a visually good job of representing the shape of the data. This supports the interpretation of the data in terms of capillary waves.

In the plots given below (Figures 5−7), the uncertainty in the parameters derived from the fits were calculated from the least-squares minimization routine.[18] This will not necessarily be an accurate measure of uncertainty in the presence of systematic errors. In some cases we find that calculated uncertainties appear smaller than the observed scatter in the results. In these cases the scatter may be a better indication of uncertainty in the parameter values.

The best fit result for the surface tension is displayed in Figure 5. The data are shown as a function of both film thickness and temperature. The uncertainty, depicted by the error bars, is dominated by the accuracy with which the data could be normalized, which was of order 10%. Since the surface tension depends on the square root of the intensity, this leads to an overall 3% uncertainty. Surface tension values were slightly higher than the bulk values[19] (shown by the solid line). The surface tension shows a similar temperature dependence as bulk PS with no systematic variation as a

function of film thickness.

The unconstrained value of q_u obtained from the fits were larger than the upper wavevector cutoff determined by the monomer size. We regard this as an unphysically large value. This large value of q_u can be interpreted as due to an excess surface roughness at small length scales, as might result from the static structure of the monomer at the surface. Consequently, q_u was constrained to be $2\pi/a = 23$ nm^{-1}. Here, a is the monomer size. In the constrained fits the intrinsic roughness σ_0 was able to compensate for the smaller value of q_u, and comparable values of χ^2 were obtained. Figure 6 displays the resulting values obtained for σ_0. These show an increase in intrinsic roughness with increasing temperature and, perhaps, a weak thickness dependence with thinner films being slightly rougher.

We now turn to a consideration of the constant background required to fit the experimental data. Results for this constant obtained from the fits are shown in Figure 7. The overall magnitude of the constant background was of order 7×10^{-5}. We hypothesize that this comes from density fluctuations within the bulk of the polystyrene. In the simplest approximation, the structure factor for scattering from bulk fluctuations is proportional to the compressibility; hence[1]

$$\frac{d\sigma}{d\Omega} = \rho_e^2 r_e^2 V |T(\alpha)|^2 |T(\beta)|^2 k_B T \beta \qquad (7)$$

Here β is the isothermal compressibility and V the sample volume. The illuminated volume is given by the area of the beam on the surface and the penetration depth of the X-rays[1]

$$V = \frac{A_{beam}}{2\mathrm{Im}(k_z^t)\sin(\theta_{in})} \qquad (8)$$

Here k_z^t is the z component of the wavevector of the transmitted X-ray beam and $^1/_2\mathrm{Im}(k_z^t)$ is the penetration depth of the X-rays. If we substitute the bulk modulus of PS (assuming a linear variation of β with temperature[20]), eqs 7 and 8 predict a static background too small by approximately a factor of 4. To test whether the constant background was actually due to bulk scattering, measurements were made at 0.2° incident angle (0.04° above the critical angle). The scattering was measured from a 388 nm film at 160 °C. The diffuse background in this case was 9 times larger than when the X-rays were incident below the critical angle. On the basis of eq 8, one would expect an increase of a factor of 15. It is suggestive that the background is due to bulk scattering The bulk scattering is, however, only proportional to the isothermal compressibility in the limit of small wavevector, and it is not clear whether we are in that limit here.

Discussion

Other experiments probing the surface roughness of highly viscous liquids have observed anomalously small surface roughness. Seydel et al.[21] have recently reported that the surface roughness of glycerol near its glass transition temperature was lower than predicted from capillary wave theory if one assumes that the experimental resolution sets the long wavelength cutoff. They were unable to account for this discrepancy. Jeng et al.[22] have observed lower than expected surface roughnesses at the interface of an oil−water−surfactant system. As mentioned above, the experiments of Wang et al.[15] found significantly less surface roughness for PS films than expected on the basis of capillary wave theory. Their study concentrated primarily on very thin films, although they measured films up to 168 nm which do overlap with the thicknesses measured here. Wang argued that the deviation might be due to a higher than expected surface tension or to a deviation from the predicted form of $g(r)$ for capillary waves. The present measurement, however, appears to find both the expected surface tension and an excess total surface roughness as compared with bulk capillary wave theory. It is possible that the discrepancy with Wang et al. arises from the present measurement being carried out in situ above T_g while their polymer films were cooled to room temperature before measurement. Perhaps a more significant difference is that Wang et al. determined the surface tension based entirely on the value of η determined from the power law decay with q_R. The present measurement chiefly used absolute intensity normalization to fix the surface tension. As pointed out by Wang et al., their small value of the surface tension could have resulted from the failure of the capillary wave model to describe $g(R)$ at small values of R (e.g., large values of q_R). The present experiment also found that the capillary wave model did not describe the data well in this region.

Conclusion

We have measured the surface diffuse scattering from a series of PS films with thickness varying from 84 to 350 nm over a range in temperatures above the PS glass transition temperature from 120 to 180 °C. Comparison of the absolute scattering intensity in the near-specular regime with the intensity expected from thermal capillary waves yields values for the surface tension that are in reasonable agreement with the bulk value. We find no evidence to support a strongly enhanced surface tension as reported by Wang et al. Capillary wave theory describes the observed diffuse scattering measured over a range of in-plane wavevector 10^{-2} nm^{-1} < q_R < 2 nm^{-1}. There appears to be an excess total surface roughness possibly due to the static structure of the polymer. Bulk scattering was found to compete with surface diffuse scattering at in-plane wavevectors greater than around 1 nm^{-1}. While it would be very interesting to study the diffuse scattering in this large wavevector regime, the difficulty of separating the bulk and diffuse scattering becomes significant. It is possible that future measurements can take advantage of the enhancement of scattering along the Yoneda peak[23] in order to resolve this issue.

Acknowledgment. We thank Jan Ilavsky and Suresh Narayanan for measurements of the absolute scattering standards used in this study. Work at MIT and Yale was supported by the NSF (DMR 0071755). J.K.B. was supported by the DOE (DEFG02-91ER45439). 8-ID is supported by the DOE Facilities Initiative Program DE-FG02-96ER45593 and NSERC. The APS is supported by the U.S. Department of Energy, Office of Basic Science, under W31-109-ENG-38.

References and Notes

(1) Fraden, C.; Braslau, A.; Luzet, D.; Smilgies, D.; Alba, M.; Boudet, N.; Mecke, K.; Daillant, J. *Nature (London)* **2000**, *403*, 871.

(2) Braslau, A.; Pershan, P. S.; Swislow, G.; Ocko, B. M.; Als-Nielsen, J. *Phys. Rev. A* **1988**, *38*, 2457.
(3) Lurio, L. B.; Rabedeau, T. A.; Pershan, P. S.; Silvera, I. F.; Deutsch, M.; Ocko, B. M.; Kosowski, S. D. *Phys. Rev. B* **1993**, *48*, 9644.
(4) Ocko, B. M.; Wu, Z. X.; Sirota, E. B.; Sinha, S. K.; Deutsch, M. *Phys. Rev. Lett.* **1994**, *72*, 242.
(5) Sanyal, M. K.; Sinha, S. K.; Huang, K. G.; Ocko, B. M. *Phys. Rev. Lett.* **1991**, *66*, 628.
(6) Penfold, J. *Rep. Prog. Phys.* **2001**, *64*, 777.
(7) McClain, B. R.; Yoon, M.; Litster, J. D.; Mochrie, S. G. J. *Eur. Phys. J. B* **1999**, *10*, 45.
(8) Müller-Buschbaum, P.; Gutmann, J. S.; Lorenz, C.; Schmitt, T.; Stamm, M. *Macromolecules* **1998**, *31*, 9265.
(9) Fredrickson, G. H.; Ajdari, A.; Leibler, L.; Carton, J. P. *Macromolecules* **1992**, *25*, 2882.
(10) Mecke, K. R.; Dietrich, S. *Phys. Rev. E* **1999**, *59*, 6766.
(11) Sinha, S. K.; Sirota, E. B.; Garoff, S. *Phys. Rev. B* **1988**, *38*, 2297.
(12) Als-Nielsen, J. *Elements of Modern X-Ray Physics*; Wiley: West Sussex, 2001.
(13) Schwartz, D. K.; Schlossman, M. L.; Kawamoto, E. H.; Kellogg, G. J.; Pershan, P. S. *Phys. Rev. A* **1990**, *41*, 5687.
(14) Tolan, M. *X-Ray Scattering from Soft-Matter Thin Films*; Springer-Verlag: Berlin, 1999.
(15) Wang, J.; Tolan, M.; Seeck, O. H.; Sinha, S. K.; Bahr, O.; Rafailovich, M. H.; Sokolov, J. *Phys. Rev. Lett.* **1999**, *83*, 564.
(16) Plazek, D. J.; O'Rourke, V. M. *J. Polym. Sci., Part A2* **1971**, *9*, 209.
(17) Mochrie, S. G. J.; Kortan, A. R.; Birgeneau, R. J. *Z. Phys. (Munich)* **1985**, *62*, 79.
(18) Bevington, P. R.; Robinson, D. K. *Data Reduction and Error Analysis for the Physical Sciences*, 2nd ed.; McGraw-Hill: New York, 1992.
(19) Brandrup, J.; Immergut, E. H. *Polymer Handbook*, 3rd ed.; John Wiley and Sons: New York, 1989.
(20) Boundy, R. H., Boyer, R. F., Eds. *Styrene Its Polymers, Copolymers and Derivatives*; Reinhold Publishing Corp.: New York, 1952.
(21) Seydel, T.; Tolan, M.; Ocko, B. M.; Seeck, O. H.; Weber, R.; DiMasi, E.; Press, W. *Phys. Rev. B* **2002**, *65*, 184207/1.
(22) Jeng, U.-S.; Esibov, L.; Crow, L.; Steyerl, A. *J. Phys.: Condens. Matter* **1998**, *10*, 4955.
(23) Yoneda, Y. *Phys. Rev.* **1963**, *131*, 2010.

MA034189L